CHEMISTRY OF MATERIALS

pubs.acs.org/cm

Article

Suppression of Auger Recombination by Gradient Alloying in InAs/CdSe/CdS QDs

Laxmi Kishore Sagar,[⊥] Golam Bappi,[⊥] Andrew Johnston, Bin Chen, Petar Todorović, Larissa Levina, Makhsud I. Saidaminov, F. Pelayo García de Arquer, Dae-Hyun Nam, Min-Jae Choi, Sjoerd Hoogland, Oleksandr Voznyy, and Edward H. Sargent*

Cite This: https://dx.doi.org/10.1021/acs.chemmater.0c01788

Read Online

ACCESS | Metrics & More | Article Recommendations | Supporting Information

ABSTRACT: Colloidal quantum dots are promising for low-cost optoelectronic devices such as solar cells, light-emitting diodes (LEDs), lasers, and photodetectors. InAs-based quantum dots (QDs) are well suited for near-infrared (NIR) applications; however, to date, the highest-QY InAs QDs have exhibited short biexciton Auger lifetimes of ∼<50 ps. Here, we report a band engineering strategy that doubles the Auger lifetime in InAs CQDs. By developing a continuously graded thick $CdSe_xS_{1-x}$ shell, we synthesize InAs/$CdSe_xS_{1-x}$/CdS CQDs that enable a smooth progression from the core to the outer shell, slowing the Auger process. We report a biexciton Auger lifetime of ∼105 ps compared to 17 ps for control InAs/CdSe/CdS CQDs. This represents a 2× increase of the Auger lifetime relative to the best value reported for InAs CQDs in prior literature.

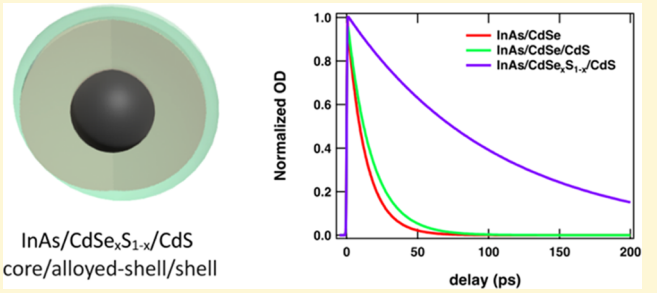

INTRODUCTION

Semiconductor quantum dots (QDs) exhibit size-dependent optoelectronic properties related to the quantum confinement effect.[1,2] Solution-processed syntheses of QDs offer a platform for flexible and large-area optoelectronic devices; QDs have been investigated in color conversion, light-emitting diodes (LEDs), photodetection, lasers, and photovoltaics.[3−6] The syntheses of II−VI and IV−VI QDs have been studied extensively, while III−V QDs show the remaining potential for further synthetic improvement.[7] The covalent bonding of III−V semiconductors compared to II−VI counterparts makes it challenging to synthesize them, often requiring higher temperatures, longer reaction times, and higher activation barriers to crystallize.[8] Recent advancements in understanding the precursor kinetics of III−V QDs have brought insights that may underpin further advances in performance.[9,10]

InAs is a III−V semiconductor with a bulk band gap of 0.35 eV and a large exciton Bohr radius (a_{ex} = 31 nm), making InAs dots well suited to near-infrared (NIR) applications.[8] However, pure InAs QDs (cores only) have a low photoluminescence quantum yield (PLQY) of 1−2% due to fast surface trapping induced by poor surface passivation and oxidation of the surface.[11] Growing an epitaxial shell (InP, CdSe, CdS, ZnS, and ZnSe)[9,12−15] improves the radiative:-nonradiative recombination ratio, increasing the potential of these QDs for light emission applications. However, higher-order nonradiative processes such as the Auger process have remained efficient, with the biexciton Auger lifetime being ∼<50 ps.[16−19] Auger recombination is an important factor hindering the performance in QD lasers, since optical gain typically requires the presence of multiple excitons, making lasing operation under CW excitation difficult.[20,21] Additionally, the Auger effect accounts for efficiency drop in LEDs at high driving currents.[22] To improve the Auger lifetimes of InAs core/shell QDs for optoelectronic applications, there is a need to improve the core/shell interfacial layer and develop band engineering strategies.

Here, we present a photophysical study comparing three classes of InAs core/shell QDs (Figure 1). We begin by overcoating InAs QDs with a lattice-matched CdSe shell to grow InAs/CdSe core/shell QDs. We chose to start with relatively small InAs QDs to grow a thick shell while keeping the final absorption/PL wave lengths within the 0.9−1 eV range. Thicker shells have been shown to result in improved Auger lifetimes relative to thinner shells due to a greater degree of charge carrier delocalization from the core into the shell.[23] By controlling shell precursor kinetics, we were able to synthesize either a sharp InAs/CdSe/CdS core/shell/shell or InAs/$CdSe_xS_{1-x}$/CdS core/progressively alloyed-shell/shell

Received: April 27, 2020
Revised: August 16, 2020
Published: August 19, 2020

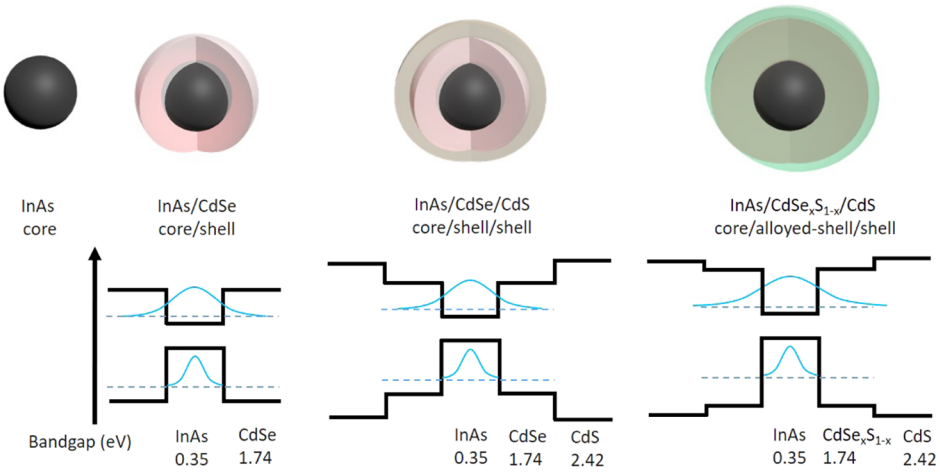

Figure 1. Band engineering strategies in InAs-based QDs. The top row shows the composition of heterostructures, and the lower panel, the band alignment. InAs/CdSe core/shell (CS) QDs have a quasi-type-II band alignment, while growth of an additional outer CdS shell leads to further confinement of carriers in InAs/CdSe/CdS core/shell/shell (CSS) QDs, alloying of an intermediate layer leads to a spatial distribution of electron and hole in InAs/$CdSe_xS_{1-x}$/CdS core/alloyed-shell/shell (CaSS) QDs.

QDs. We improve the Auger lifetime by ∼5× in the continuously graded QDs compared with control InAs/CdSe/CdS QDs with an abrupt confinement potential.

EXPERIMENTAL SECTION

Chemicals. Indium(III) acetate ($In(OAc)_3$, 99.99%), oleic acid (OA, tech., 90%), selenium powder (Se, 99.999%), cadmium oxide (CdO, 99.99%), tetrachloroethylene (C_2Cl_4, 99%), hexane (reagent grade, >99%), oleylamine (≥98%), and 1-butanol (anhydrous, 99.8%) were purchased from Sigma-Aldrich. 1-Octadecene (ODE, tech., 90%) was purchased from Alfa Aesar. Tri-*n*-octylphosphine (TOP, 97%) and sulfur powder (S, 99%) were purchased from Strem Chemicals. Anhydrous ethanol, acetone, and *n*-octane were purchased from Caledon. Tris(trimethylgermyl)arsine ($(TMGe)_3As$, 95%) was purchased from Nanomeps. All of the chemicals were used without further purification unless stated otherwise. ODE was degassed under vacuum overnight in a Schlenk flask at 110 °C. Oleylamine was degassed under vacuum for 3 h at 110 °C. Then, flasks were transferred to a glovebox for use at a later step.

InAs QD Synthesis. InAs QDs were synthesized by following the procedure of Sagar et al.[11] Purified InAs QDs were stored in a glovebox for further use. All of the core/shell QDs were synthesized starting from the same InAs core QDs.

InAs/CdSe QD Synthesis. The synthesis was carried out by modifying the approach of Franke et al.[9] In a typical synthesis, purified InAs QDs (1 mL of QDs, ≈50 mg/mL) in octane were added to a mixture of 4 mL of ODE and 4 mL of oleylamine in a Schlenk flask. The solution was degassed under vacuum at room temperature for 15 min and another 30 min at 110 °C to remove *n*-octane. Subsequently, the flow was switched to nitrogen and the solution was heated to 270 °C for the shell growth. Once the temperature reached around 240 °C, Cd-oleate (2.5 mL of Cd-oleate stock solution + 1.5 mL of ODE) and TOP-Se (1 mL of TOP-Se + 1 mL of ODE) shell precursors were added in a dropwise fashion over 60 min. We monitored CdSe shell growth by taking aliquots throughout the growth process and measuring the absorption and PL spectra. Once the desired CdSe shell thickness was achieved, the solution was cooled down to room temperature for the purification of the dots. Hexane and 1-butanol + acetone were used as solvent and antisolvent, respectively. After two purification cycles, the QDs were dispersed in *n*-octane. Purification of InAs/CdSe QDs was done under ambient conditions as follows: 5.4 nm sized InAs/CdSe QDs were characterized by an absorption at 1.14 eV and PL at 1.04 eV; 6.7 nm sized InAs/CdSe QDs were characterized by an absorption at 1.01 eV and PL at 0.94 eV.

InAs/CdSe/CdS QD Synthesis. Purified InAs/CdSe QDs were used as seeds to grow the CdS shell. In a Schlenk flask, 4 mL of ODE and 4 mL of oleylamine were added to InAs/CdSe QDs. The solution was degassed under vacuum for 15 min at room temperature and another 30 min at 110 °C to remove the solvent. Subsequently, the flow was switched to nitrogen and the solution was heated to 270 °C for the shell growth. Once the temperature reached 240 °C, Cd-oleate (3 mL of Cd-oleate stock solution + 2 mL of ODE) and TOP-S (1.5 mL of TOP-Se + 1 mL of ODE) shell precursors were added in a dropwise fashion over 60 min. After CdS shell growth, the solution was cooled down to room temperature for the purification of the dots. Hexane and 1-butanol + acetone were used as solvent and antisolvent, respectively. After two purification cycles, the QDs were dispersed in *n*-octane. Two different InAs/CdSe/CdS QDs with similar final volumes were synthesized by varying CdSe and CdS shell thicknesses.

InAs/$CdSe_xS_{1-x}$/CdS QD Synthesis. The entire synthesis was carried out in a single step. An approach similar to that for InAs/CdSe QDs was used, except that both TOP-Se + TOP-S were mixed together, and Cd-oleate were injected at 270 °C over 90 min. After the growth of $CdSe_xS_{1-x}$ shell, an outer CdS shell growth was carried out. The same purification cycles as mentioned above were used.

Shell Precursor Stock Solutions. *Cd-Oleate Stock Solution.* CdO (0.520 g), 10 mL of oleic acid, and 54 mL of ODE were taken in a round-bottomed flask and evacuated under vacuum at 110 °C for 90 min. The flow was switched to nitrogen, and the flask was heated to 200 °C until the solution became clear. The flask was cooled down to room temperature and transferred to a glovebox for further use.

Synthesis of TOP-Se. A saturated TOP-Se solution was prepared by mixing and stirring 1.78 g of selenium powder in 10 mL of TOP inside a glovebox.

Synthesis of TOP-S. A saturated TOP-S solution was prepared by stirring 0.72 g of sulfur powder in 10 mL of TOP inside a glovebox.

Absorption Measurements. The optical absorption measurements were performed with a PerkinElmer Lambda 950 UV−vis−NIR spectrophotometer. The solutions were placed in a quartz cuvette with a 1 mm path length. The absorption measurements were done by evaporating the initial *n*-octane under a constant flow of nitrogen using a nitrogen gun and then redispersing the dots in C2Cl4 prior to the measurement.

Photoluminescence Quantum Yield (PLQY) Measurements. The steady-state photoluminescence measurements were performed using a Horiba Fluorolog time-correlated single-photon counting system equipped with UV/vis/NIR photomultiplier detectors, dual grating spectrometers, and a monochromatized xenon lamp as an excitation source. The samples were excited at 700 nm using a 500 W xenon lamp. The published method was used for measuring quantum

https://dx.doi.org/10.1021/acs.chemmater.0c01788
Chem. Mater. XXXX, XXX, XXX−XXX

yields in an integrating sphere.[24] Light was coupled into the Fluorolog system and the integrating sphere with optical fiber bundles. Time-resolved PL measurements were performed by exciting the samples with a 723 nm laser. The fluence is sufficiently low such that only single excitons are present in the samples after photoexcitation.

Ultrafast Transient Absorption Spectroscopy. A regeneratively amplified Yb:KGW laser (PHAROS, Light Conversion) was used to generate femtosecond pulses (250 fs, FWHM) at 1030 nm as the fundamental beam with a 5 kHz repetition rate. This fundamental beam was passed through a beam splitter, where one arm was used to pump an optical parametric amplifier (ORPHEUS, Light Conversion) for the narrowband pump and the other arm was focused into a sapphire crystal (Ultrafast Systems) to generate an NIR white-light continuum probe with a spectral window of 1050−1600 nm. Both arms were directed into a commercial transient absorption spectrometer (Helios, Ultrafast Systems). The probe pulse was delayed relative to the pump pulse to provide a time window of up to 8 ns.

X-ray Photoelectron Spectroscopy (XPS). XPS spectra were measured using a Thermo Scientific K-Alpha system with an Al Kα source. The films were prepared on glass substrates. A 50 eV pass energy and scans were taken at 0.05 eV steps. The atomic ratios were obtained by integrating under the area of each peak and scaled by atomic sensitivity factors. We normalized all of the element areas with indium to obtain accurate atomic ratios.

TEM Measurement. All transmission electron microscopy (TEM) images were acquired on a Hitachi HF 3300 electron microscope operating at 300 keV. High-angle annular dark-field (HAADF) images were recorded in scanning TEM mode with a spot size of 0.7 nm and a camera length of 60 cm. TEM samples were prepared by drop-casting a purified solution of QDs from hexanes onto a 300-mesh copper grid with a carbon film (SPI supplies). ImageJ was employed to generate the size of the dots.

XRD Measurement. XRD samples were prepared by drop-casting a layer of the desired core or core−shell material from octane solution on a glass substrate. Measurements were performed on a Rigaku powder diffractometer.

RESULTS AND DISCUSSION

The as-synthesized InAs core-only QDs often exhibit poor optical performance as evidenced by their fast biexciton Auger lifetimes and low PLQYs.[17,18] As in other semiconductor quantum-confined materials,[7] these dots are associated with dangling bonds, surface defects, and incomplete surface passivation.[25] Overgrowth of a wide-band-gap shell on the QDs is used to improve surface passivation. In the case of InAs QDs, several wider-band-gap shells such as CdSe, ZnSe, CdS, and ZnS have been explored.[12,13] To achieve high optical performance and eliminate defects at the core/shell interface, it is important to keep the lattice mismatch as low as possible. In this work, CdSe-based shells are chosen as the epitaxial shells since InAs shares the same zinc blende crystal structure and has minimal lattice mismatch.[12]

To investigate the optical properties and photophysics of InAs-Cd-based core/shell QDs, we chose three different core/shell structures with similar excitonic wave lengths. Figure 1 shows the schematic and approximate band alignment of the different core/shell QDs used in this work. Simulations of the electron and hole wave functions were performed using COMSOL and are included in the Supporting Information (Figure S1). InAs/CdSe CS QDs offer a simple heterostructure with a quasi-type-II band alignment.[9] An outer CdS shell was chosen to grow onto InAs/CdSe QDs to further confine the charge carriers, resulting in InAs/CdSe/CdS CSS QDs. The synthesis was achieved in a two-step manner with an intentional sharp interface between CdSe and CdS. To engineer the band structure further, another sample was synthesized wherein we intentionally introduced a smooth alloyed interface to make InAs/CdSe$_x$S$_{1-x}$/CdS CaSS QDs. This was achieved by preheating InAs QDs in a mixture of oleylamine and ODE at 270 °C by continually supplying Cd and Se + S sources together (see Experimental Secion).

Figure 2a,b shows the evolution of absorption and photoluminescence (PL) spectra of InAs QDs during the

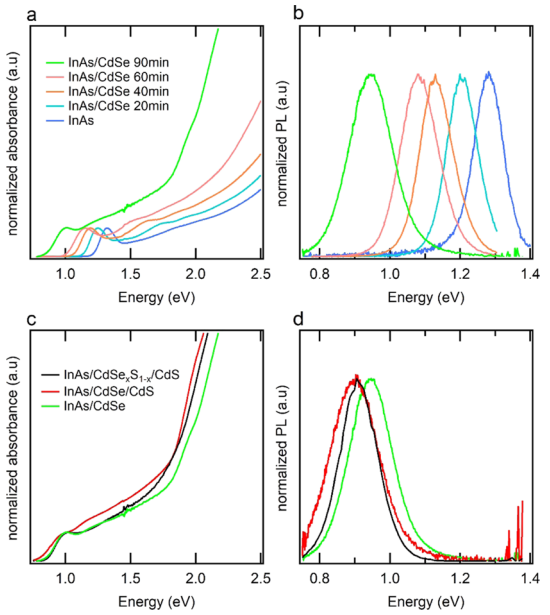

Figure 2. Optical characterization of InAs-based core/shell QDs. (a, b) Evolution of absorption and photoluminescence spectra of 3.1 nm size InAs core QDs during the CdSe shell growth. A red shift of absorption and PL spectra upon the growth of CdSe onto InAs core QDs is indicative of quasi-type-II band alignment. (c, d) Absorption and photoluminescence spectra of InAs/CdSe (CS), InAs/CdSe/CdS (CSS), and InAs/CdSe$_x$S$_{1-x}$/CdS (CaSS) QDs.

CdSe shell growth. The absorption spectra of InAs core QDs show a band-edge exciton transition at 1.32 eV as well as higher energy features; the concomitant PL emission centered at 1.28 eV with a PLQY of 1%. CdSe shell growth resulted in a gradual shift in the absorption and PL toward lower energies suggesting a quasi-type-II heterostructure.[9,26] CdSe shell growth was further confirmed by the marked increase in the absorbance at energies well below the band gap of bulk CdSe. Additionally, InAs/CdSe QDs exhibited an increased PLQY of 20%, indicative of improved surface passivation. Even though CdSe shell growth provides minimum lattice mismatch, the electron delocalization into the shell leads to increased radiative lifetimes and limits the efficiency of PLQYs.[9] To compare photophysics of the three different core/shell structures, we choose to work with QDs with similar absorption and PL wave lengths, to exclude the effects of QD volume on Auger lifetime. Figure 2c,d shows the absorption and PL of InAs/CdSe, InAs/CdSe/CdS, and InAs/CdSe$_x$S$_{1-x}$/CdS QDs under investigation. Additionally, there is a marked increase in absorption at shorter wave lengths below the band gap of CdSe and CdS, indicating the shell growth (Figure S2).

Figure 3 shows transmission electron microscopy (TEM) images of InAs core and InAs core/shell QDs. Bright-field TEM (Figure 3a) and high-resolution TEM (HR-TEM)

https://dx.doi.org/10.1021/acs.chemmater.0c01788
Chem. Mater. XXXX, XXX, XXX−XXX

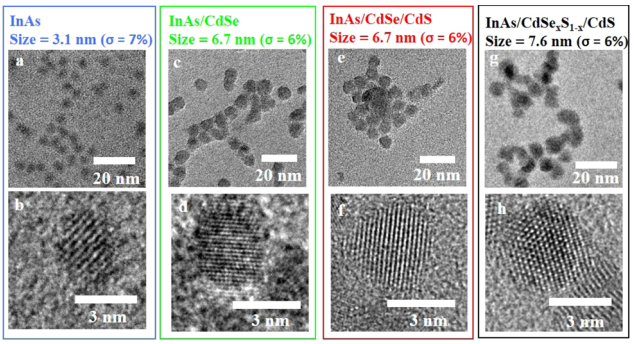

Figure 3. Transmission electron microscopy (TEM) images of InAs core, InAs/CdSe, InAs/CdSe/CdS, and InAs/$CdSe_xS_{1-x}$/CdS QDs. (a, c, e, and g) Bright-field TEM images of InAs core, InAs/CdSe, InAs/CdSe/CdS, and InAs/$CdSe_xS_{1-x}$/CdS, respectively. (b, d, f, and h) HR-TEM images of the same showing lattice fringes and single coherent lattice.

(Figure 3b) images confirm that the starting InAs core QDs have quasi-spherical morphology with an estimated size of 3.1 nm. After shell growth, there is an increase in overall size of the dots; InAs/CdSe QDs are 6.7 nm, InAs/CdSe/CdS QDs are 6.7 nm, and InAs/$CdSe_xS_{1-x}$/CdS are 7.6 nm, while the quasi-spherical morphology is retained (Figure 3c,e,g). HR-TEM images (Figure 3d,f,h) of core/shell QDs show well-defined lattice fringes, suggesting the high crystallinity of QDs and all core/shell QDs. A single coherent lattice indicates that the shell growth is epitaxial. Size histograms of InAs core and InAs core/shell QDs are provided in Figure S3. High-angle annular dark-field scanning transmission electron microscopy (HAADF-STEM) line scan and energy-dispersive X-ray spectroscopy (EDS) confirm the elemental composition of each sample (see Supporting Information Figure S4). In particular, the line scan of InAs/$CdSe_xS_{1-x}$/CdS QDs shows the presence of the Se and S peaks in the center of the nanocrystal, suggesting the alloying of the shell. The estimated composition is $CdSe_{0.69}S_{0.31}$. In the case of InAs/CdSe/CdS QDs, the Se peak is located in the center while the S peak is at the edge of the nanocrystal. Further evidence of shell growth is shown in X-ray photoelectron spectroscopy (XPS) survey spectra, high-resolution spectra, and elemental analysis (see Figure S5 and Table S1). Taking together the EDX and XPS elemental composition analyses, we conclude that In and As are indeed present in InAs QDs and In, As, Cd, Se, and S are present in InAs/CdSe; we observe In, As, Cd, Se, and S with a sharp interface in the case of InAs/CdSe/CdS and In, As, Cd, Se, and S with a smooth graded interface in InAs/$CdSe_xS_{1-x}$/CdS. XPS of InAs core QDs indicates the oxidation of As 3d, resulting in As_2O_3 under ambient conditions, whereas upon growth of shells, As_2O_3 is not seen even when the samples are stored under ambient conditions—a finding consistent with our observation of surface passivation (see Figure S5). Figure S6 compares the X-ray diffraction patterns of InAs core QDs and InAs core/shell QDs: the peak positions of InAs core QDs match the bulk InAs zinc blende structure. After overgrowth of shells, there is no change in the XRD peak position, indicating the retention of zinc blende crystal structure and lattice-

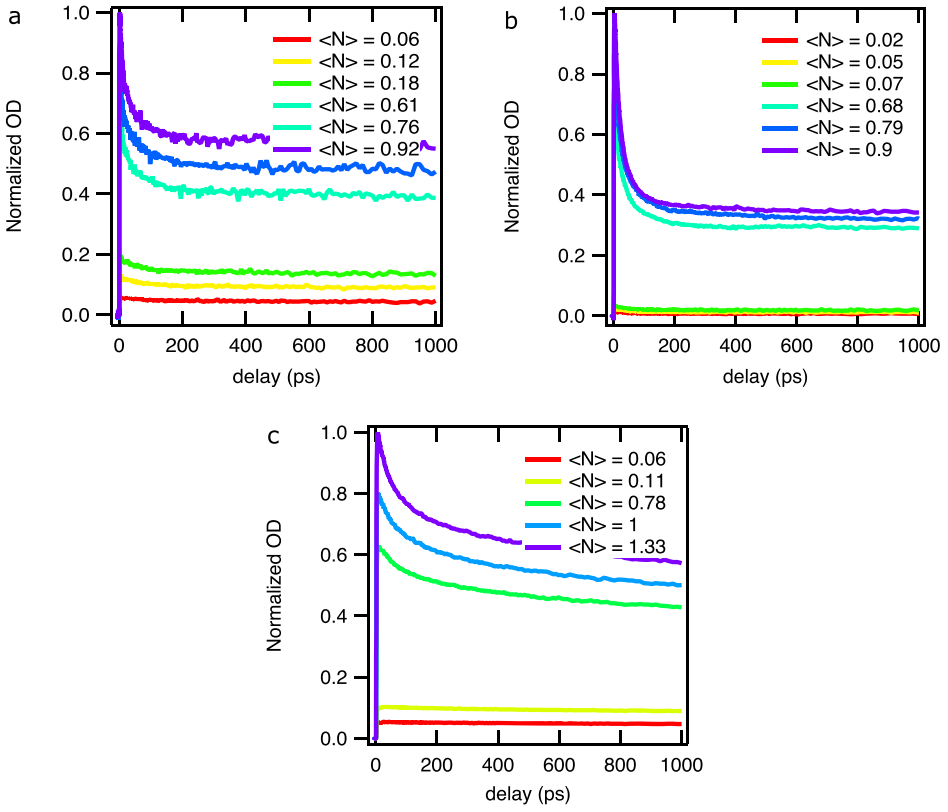

Figure 4. Ultrafast spectroscopy of QDs. Power-dependent bleach kinetic traces for (a) InAs/CdSe, (b) InAs/CdSe/CdS, and (c) the smoothly graded InAs/$CdSe_xS_{1-x}$/CdS CQD samples. The slower biexciton decay of the graded sample in (c) relative to (a) and (b) demonstrates the substantial benefits of smoothening the confinement potential of the carriers. The probe wave lengths are (a) 0.986 eV, (b) 0.963 eV, and (c) 0.950 eV.

https://dx.doi.org/10.1021/acs.chemmater.0c01788
Chem. Mater. XXXX, XXX, XXX−XXX

matched core/shell QDs.[12] The (111) peak is considerably narrower in the InAs core/shell QDs, confirming the increase in crystal size, which is consistent with TEM analysis. We conclude from our structural and elemental analyses that our samples were synthesized with the desired core/shell architectures.

We sought to understand the photophysical properties of the different InAs QD systems: we utilize transient absorption spectroscopy (TAS) to investigate the power-dependent carrier kinetics in each sample. Figure 4a−c shows the power-dependent bleach kinetic traces for the three samples of InAs/CdSe, InAs/CdSe/CdS, and InAs/$CdSe_xS_{1-x}$/CdS CQDs. As the excitation intensity is increased, a second, faster, decay component emerges, and this is assigned to biexciton Auger recombination.[27] We plot the long-time (∼7 ns) bleach value as a function of pump fluence and fit to $B = B_0\ (1 - \exp(-\langle N\rangle))$, in which $\langle N\rangle$ is the average number of excitons per dot created after photoexcitation.[28] We determine the average number of excitons per dot generated at each pump power assuming Poisson statistics (Figure S7).[29]

Multiphoton absorption is negligible at low pump fluences ($\langle N\rangle \sim 0.1$), and the dynamics are dominated by that of single excitons. At higher pump fluences ($\langle N\rangle \sim 1$), a fast biexciton decay component is evident in the bleach kinetics. To determine the lifetimes of the various processes, we used multiexponential fittings at each pump fluence, which allowed us to extract the biexciton Auger lifetime (summarized in Table 1).

Table 1. Summary of Auger Lifetimes of Various Samples

sample	PL peak (eV)	Biexciton Auger lifetime (ps)	PLQY (%)
InAs/CdSe	0.94	13 ± 0.5	20
InAs/CdSe/CdS	0.91	17 ± 1	24
InAs/$CdSe_xS_{1-x}$/CdS	**0.94**	**105 ± 3**	**30**

The InAs/CdSe sample exhibited a biexciton Auger lifetime of 13 ± 0.5 ps, which is similar to values previously reported in the literature.[17] At low pump fluences, the bleach decay is due to trap-assisted Auger recombination.[30] With trap-assisted Auger recombination, an excitonic electron or hole fills a trap state near the conduction or valence band respectively, with the energy being transferred to the other band-edge carrier. These decay processes are summarized in Table S2. The InAs/CdSe/CdS sample exhibited a similar biexciton Auger lifetime of 17 ± 1 ps, while the continuously graded CdSe/$CdSe_xS_{1-x}$/CdS sample had a record biexciton Auger lifetime of 105 ± 3 ps. We attribute the 5-fold increase in biexciton Auger lifetime to smoothing the confinement potential of the carriers.[31] Given that InAs/CdSe exhibits a quasi-type-II band alignment with a small conduction band offset, the CdSe shell results in delocalization of the electron wave function.[9] This is expected to reduce the Auger rate due to reduced Coulomb interactions within the quantum dot. However, when we compare the samples with an abrupt and smoothened CdSe/CdS shell, we observe the positive influence of grading the confinement potential. Varying the shell thickness of the CdSe (Figure S8, Table S3) or final CdS (Figure S9, Table S4) layer, and hence the degree of carrier delocalization, did not improve the Auger lifetime. Only by grading the CdSe/CdS interfacial layer were we able to suppress the Auger recombination process. This result is consistent with Cragg and Efros' theory that the overlap between the initial and final states of the excited carrier during Auger recombination is decreased when the confinement potential is smooth and not abrupt.[31]

CONCLUSIONS

We studied the influence of the core/shell confinement potential on the biexciton Auger recombination rate in InAs core/shell QDs. We find that the Auger lifetime can be extended up to 5 times by alloying the CdSe/CdS interface to smoothen the carrier confinement potential. Power-dependent transient absorption spectroscopy was used to investigate single-exciton and biexciton dynamics. This revealed that the single-exciton dynamics are dominated by trap-assisted Auger recombination.[30] At higher fluences, the biexciton lifetime can be extracted to reveal the drastic increase when the confining potential is smoothened. Electron delocalization due to shell growth alone is not enough to observe this improvement. This work reports the first continuously graded shelling of InAs QDs is one step in the direction of InAs-based LEDs and lasers.

ASSOCIATED CONTENT

Supporting Information

The Supporting Information is available free of charge at https://pubs.acs.org/doi/10.1021/acs.chemmater.0c01788.

Information on the absorption spectra of InAs core, InAs/CdSe, and InAs/$CdSe_xS_{1-x}$/CdS; size histograms; high-angle annular dark-field scanning transmission electron microscopy (HAADF-STEM) line scan and energy-dispersive X-ray spectroscopy (EDS) analysis; XPS results of InAs core, InAs/CdSe, InAs/CdSe/CdS, and InAs/$CdSe_xS_{1-x}$/CdS; X-ray diffraction studies (XRD); determination of the exciton population; electron and hole wave functions of InAs core/shell samples; 5.4 nm sized InAs/CdSe core/shell QD characterization; 6.7 nm sized InAs/CdSe/CdS core/shell/shell QD characterization; determination of exciton population in a InAs core/shell sample; summary of exciton decay processes at $\langle N\rangle \sim 1$ for InAs core/shell samples; electron and hole wave function distributions in InAs/CdSe, InAs/CdSe/CdS, and InAs/$CdSe_xS_{1-x}$/CdS quantum dots (PDF)

AUTHOR INFORMATION

Corresponding Author

Edward H. Sargent − *Department of Electrical and Computer Engineering, University of Toronto, Toronto, Ontario M5S 3G4, Canada;* orcid.org/0000-0003-0396-6495; Email: ted.sargent@utoronto.ca

Authors

Laxmi Kishore Sagar − *Department of Electrical and Computer Engineering, University of Toronto, Toronto, Ontario M5S 3G4, Canada;* orcid.org/0000-0002-7656-7308

Golam Bappi − *Department of Electrical and Computer Engineering, University of Toronto, Toronto, Ontario M5S 3G4, Canada*

Andrew Johnston − *Department of Electrical and Computer Engineering, University of Toronto, Toronto, Ontario M5S 3G4, Canada;* orcid.org/0000-0002-4545-532X

Bin Chen − *Department of Electrical and Computer Engineering, University of Toronto, Toronto, Ontario M5S 3G4, Canada*

https://dx.doi.org/10.1021/acs.chemmater.0c01788
Chem. Mater. XXXX, XXX, XXX−XXX

Petar Todorović − *Department of Electrical and Computer Engineering, University of Toronto, Toronto, Ontario M5S 3G4, Canada;* orcid.org/0000-0002-2838-876X
Larissa Levina − *Department of Electrical and Computer Engineering, University of Toronto, Toronto, Ontario M5S 3G4, Canada*
Makhsud I. Saidaminov − *Department of Electrical and Computer Engineering, University of Toronto, Toronto, Ontario M5S 3G4, Canada; Department of Chemistry and Electrical & Computer Engineering, Centre for Advanced Materials and Related Technologies (CAMTEC), University of Victoria, Victoria, British Columbia V8P 5C2, Canada;* orcid.org/0000-0002-3850-666X
F. Pelayo García de Arquer − *Department of Electrical and Computer Engineering, University of Toronto, Toronto, Ontario M5S 3G4, Canada;* orcid.org/0000-0003-2422-6234
Dae-Hyun Nam − *Department of Energy Science and Engineering, Daegu Gyeongbuk Institute of Science & Technology (DGIST), Daegu 42988, Republic of Korea;* orcid.org/0000-0002-0871-1355
Min-Jae Choi − *Department of Electrical and Computer Engineering, University of Toronto, Toronto, Ontario M5S 3G4, Canada; Department of Chemical and Biochemical Engineering, Dongguk University, Seoul 04620, Republic of Korea*
Sjoerd Hoogland − *Department of Electrical and Computer Engineering, University of Toronto, Toronto, Ontario M5S 3G4, Canada;* orcid.org/0000-0002-3099-585X
Oleksandr Voznyy − *Department of Physical and Environmental Sciences, University of Toronto, Toronto, Ontario M5S 3G4, Canada;* orcid.org/0000-0002-8656-5074

Complete contact information is available at: https://pubs.acs.org/10.1021/acs.chemmater.0c01788

Author Contributions

[⊥]L.K.S. and G.B. contributed equally to this work.

Notes

The authors declare no competing financial interest.

■ ACKNOWLEDGMENTS

This research was supported by the Ontario Research Fund-Research Excellence Program and by the Natural Sciences and Engineering Research Council (NSERC) of Canada.

■ REFERENCES

(1) Reed, M. A.; Randall, J. N.; Aggarwal, R. J.; Matyi, R. J.; Moore, T. M.; Wetsel, A. E. Observation of Discrete Electronic States in a Zero-Dimensional Semiconductor Nanostructure. *Phys. Rev. Lett.* **1988**, *60*, 535−537.
(2) Kippeny, T.; Swafford, L. A.; Rosenthal, S. J. Semiconductor Nanocrystals: A Powerful Visual Aid for Introducing the Particle in a Box. *J. Chem. Educ.* **2002**, *79*, 1094−1100.
(3) Kagan, C. R.; Lifshitz, E.; Sargent, E. H.; Talapin, D. V. Building Devices from Colloidal Quantum Dots. *Science* **2016**, *353*, No. aac5523.
(4) Carey, G. H.; Abdelhady, A. L.; Ning, Z.; Thon, S. M.; Bakr, O. M.; Sargent, E. H. Colloidal Quantum Dot Solar Cells. *Chem. Rev.* **2015**, *115*, 12732−12763.
(5) Geiregat, P.; Van Thourhout, D.; Hens, Z. A Bright Future for Colloidal Quantum Dot Lasers. *NPG Asia Mater.* **2019**, *11*, No. 41.
(6) García De Arquer, F. P.; Armin, A.; Meredith, P.; Sargent, E. H. Solution-Processed Semiconductors for Next-Generation Photodetectors. *Nat. Rev. Mater.* **2017**, *2*, No. 16100.
(7) Kovalenko, M. V.; Manna, L.; Cabot, A.; Hens, Z.; Talapin, D. V.; Kagan, C. R.; Klimov, V. I.; Rogach, A. L.; Reiss, P.; Milliron, D. J.; et al. Prospects of Nanoscience with Nanocrystals. *ACS Nano* **2015**, *9*, 1012−1057.
(8) Reiss, P.; Carrière, M.; Lincheneau, C.; Vaure, L.; Tamang, S. Synthesis of Semiconductor Nanocrystals, Focusing on Nontoxic and Earth-Abundant Materials. *Chem. Rev.* **2016**, *116*, 10731−10819.
(9) Franke, D.; Harris, D. K.; Chen, O.; Bruns, O. T.; Carr, J. A.; Wilson, M. W. B.; Bawendi, M. G. Continuous Injection Synthesis of Indium Arsenide Quantum Dots Emissive in the Short-Wavelength Infrared. *Nat. Commun.* **2016**, *7*, No. 12749.
(10) Srivastava, V.; Dunietz, E.; Kamysbayev, V.; Anderson, J. S.; Talapin, D. V. Monodisperse InAs Quantum Dots from Aminoarsine Precursors: Understanding the Role of Reducing Agent. *Chem. Mater.* **2018**, *30*, 3623−3627.
(11) Sagar, L. K.; Bappi, G.; Johnston, A.; Chen, B.; Todorović, P.; Levina, L.; Saidaminov, M. I.; García de Arquer, F. P.; Hoogland, S.; Sargent, E. H. Single-Precursor Intermediate Shelling Enables Bright, Narrow Line Width InAs/InZnP-Based QD Emitters. *Chem. Mater.* **2020**, *32*, 2919−2925.
(12) Cao, Y. W.; Banin, U. Growth and Properties of Semiconductor Core/Shell Nanocrystals with InAs Cores. *J. Am. Chem. Soc.* **2000**, *122*, 9692−9702.
(13) Cao, Y. W.; Banin, U. Synthesis and Characterization of InAs/InP and InAs/CdSe Core/Shell Nanocrystals. *Angew. Chem.* **1999**, *38*, 3692−3694.
(14) Aharoni, A.; Mokari, T.; Popov, I.; Banin, U. Synthesis of InAs/CdSe/ZnSe Core/Shell1/Shell2 Structures with Bright and Stable Near-Infrared Fluorescence. *J. Am. Chem. Soc.* **2006**, *128*, 257−264.
(15) Xie, R.; Chen, K.; Chen, X.; Peng, X. InAs/InP/ZnSe Core/Shell/Shell Quantum Dots as Near-Infrared Emitters: Bright, Narrow-Band, Non-Cadmium Containing, and Biocompatible. *Nano Res.* **2008**, *1*, 457−464.
(16) Pijpers, J. J. H.; Hendry, E.; Milder, M. T. W.; Fanciulli, R.; Savolainen, J.; Herek, J. L.; Vanmaekelbergh, D.; Ruhman, S.; Mocatta, D.; Oron, D.; et al. Carrier Multiplication and Its Reduction by Photodoping in Colloidal InAs Quantum Dots. *J. Phys. Chem. C* **2007**, *111*, 4146−4152.
(17) Schaller, R. D.; Pietryga, J. M.; Klimov, V. I. Carrier Multiplication in InAs Nanocrystal Quantum Dots with an Onset Defined by the Energy Conservation Limit. *Nano Lett.* **2007**, *7*, 3469−3476.
(18) Ben-Lulu, M.; Mocatta, D.; Bonn, M.; Banin, U.; Ruhman, S. On the Absence of Detectable Carrier Multiplication in a Transient Absorption Study of InAs/CdSe/ZnSe Core/Shell1/Shell2 Quantum Dots. *Nano Lett.* **2008**, *8*, 1207−1211.
(19) Pijpers, J. J. H.; Milder, M. T. W.; Delerue, C.; Bonn, M. Multi)exciton Dynamics and Exciton Polarizability in Colloidal InAs Quantum Dots. *J. Phys. Chem. C* **2010**, *114*, 6318−6324.
(20) Klimov, V. I.; Mikhailovsky, A. A.; Xu, S.; Malko, A. A.; Hollingsworth, J. A.; Leatherdale, C. A.; Eisler, H. J.; Bawendi, M. G. Optical Gain and Stimulated Emission in Nanocrystal Quantum Dots. *Science* **2000**, *290*, 314−317.
(21) Fan, F.; Voznyy, O.; Sabatini, R. P.; Bicanic, K. T.; Adachi, M. M.; McBride, J. R.; Reid, K. R.; Park, Y. S.; Li, X.; Jain, A.; et al. Continuous-Wave Lasing in Colloidal Quantum Dot Solids Enabled by Facet-Selective Epitaxy. *Nature* **2017**, *544*, 75−79.
(22) Anikeeva, P. O.; Madigan, C. F.; Halpert, J. E.; Bawendi, M. G.; Bulović, V. Electronic and Excitonic Processes in Light-Emitting Devices Based on Organic Materials and Colloidal Quantum Dots. *Phys. Rev. B* **2008**, *78*, No. 085434.
(23) García-Santamaría, F.; Chen, Y.; Vela, J.; Schaller, R. D.; Hollingsworth, J. A.; Klimov, V. I. Suppressed Auger Recombination in "Giant" Nanocrystals Boosts Optical Gain Performance. *Nano Lett.* **2009**, *9*, 3482−3488.
(24) De Mello, J. C.; Wittmann, H. F.; Friend, R. H. An Improved Experimental Determination of External Photoluminescence Quantum Efficiency. *Adv. Mater.* **1997**, *9*, 230−232.

(25) Houtepen, A. J.; Hens, Z.; Owen, J. S.; Infante, I. On the Origin of Surface Traps in Colloidal II-VI Semiconductor Nanocrystals. *Chem. Mater.* **2017**, *29*, 752−761.
(26) Bertram, S. N.; Spokoyny, B.; Franke, D.; Caram, J. R.; Yoo, J. J.; Murphy, R. P.; Grein, M. E.; Bawendi, M. G. Single Nanocrystal Spectroscopy of Shortwave Infrared Emitters. *ACS Nano* **2019**, *13*, 1042−1049.
(27) Klimov, V. I.; Mikhailovsky, A. A.; McBranch, D. W.; Leatherdale, C. A.; Bawendi, M. G. Quantization of Multiparticle Auger Rates in Semiconductor Quantum Dots. *Science* **2000**, *287*, 1011−1013.
(28) Castañeda, J. A.; Nagamine, G.; Yassitepe, E.; Bonato, L. G.; Voznyy, O.; Hoogland, S.; Nogueira, A. F.; Sargent, E. H.; Cruz, C. H. B.; Padilha, L. A. Efficient Biexciton Interaction in Perovskite Quantum Dots under Weak and Strong Confinement. *ACS Nano* **2016**, *10*, 8603−8609.
(29) Klimov, V. I. Optical Nonlinearities and Ultrafast Carrier Dynamics in Semiconductor Nanocrystals. *J. Phys. Chem. B* **2000**, *104*, 6112−6123.
(30) Quintero-Bermudez, R.; Sabatini, R. P.; Lejay, M.; Voznyy, O.; Sargent, E. H. Small-Band-Offset Perovskite Shells Increase Auger Lifetime in Quantum Dot Solids. *ACS Nano* **2017**, *11*, 12378−12384.
(31) Cragg, G. E.; Efros, A. L. Suppression of Auger Processes in Confined Structures. *Nano Lett.* **2010**, *10*, 313−317.

https://dx.doi.org/10.1021/acs.chemmater.0c01788
Chem. Mater. XXXX, XXX, XXX−XXX